Seismic noise studies at Limburg

a candidate site for Einstein Telescope

Soumen Koley
Maria Bader
Jo van den Brand
Henk Jan Bulten
Xander Campman
Frank Linde
Bjorn Vink

Nikhef, Amsterdam
skoley@nikhef.nl

ET 11th Annual Meeting
December 2, 2020

Contents

- Measurements overview

- Surface seismic array:
  - **Phase velocity**
  - **Direction of propagation**

- Borehole studies

- 1D S-wave subsurface model

- Active seismic survey
  - **Seismic refraction tomography**

- Underground seismic noise
  - **H-V ratio**
  - **Microseismic, anthropogenic variation**
  - **Attenuation**
  - **Body wave background**

- Newtonian noise estimation

All work reported here are based on:

- Phd Thesis S. Koley, VU Amsterdam
- Phd Thesis M. Bader, VU Amsterdam, in preparation

Studies of quality at potential B-G-NL site

The geology of the B-G-NL Limburg border area: hard rock with on top a layer of soft absorbing and damping soil. In addition the region is free of disturbing (human-made) seismic activities
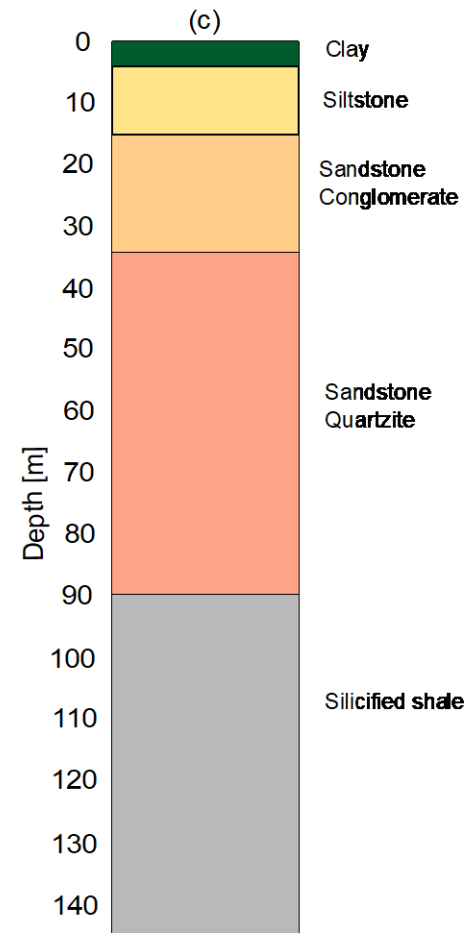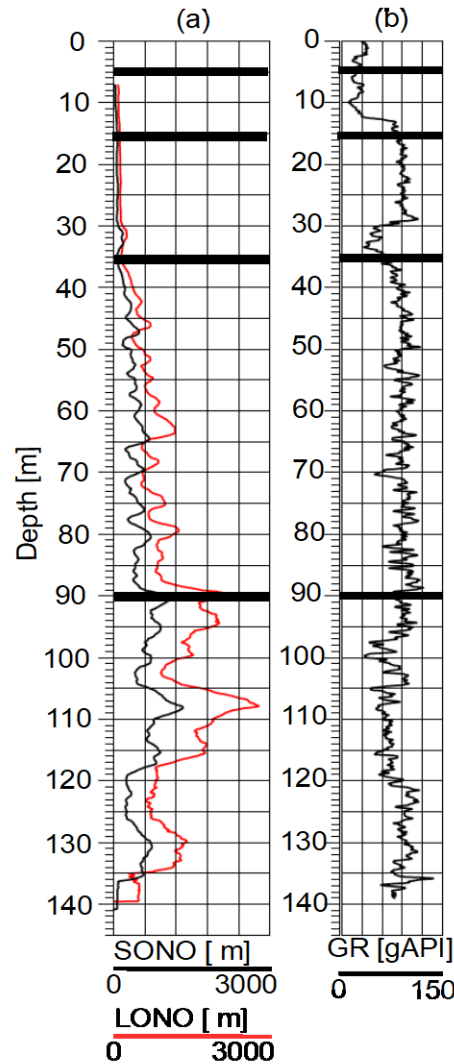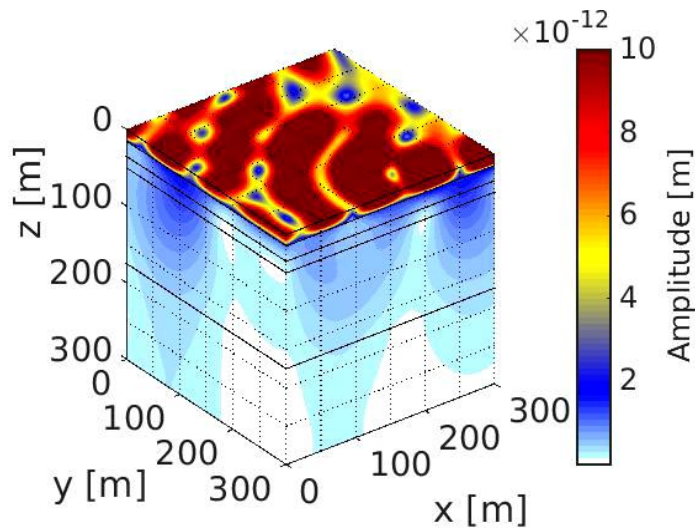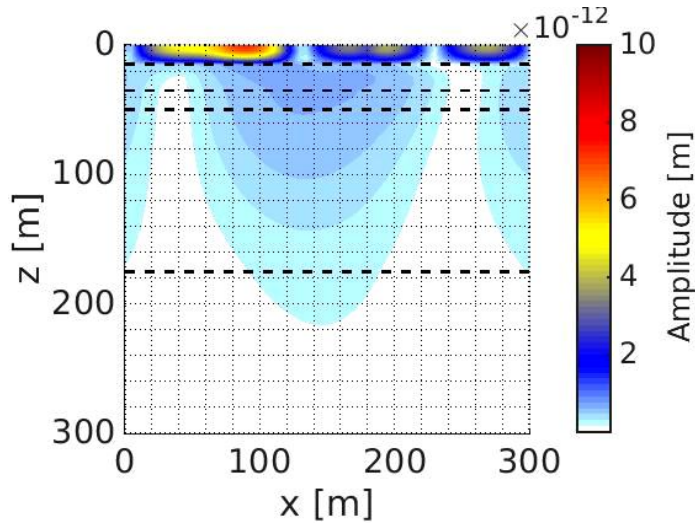
Resistivity log   Gamma ray

Lithology model

3

Surface seismic noise characteristics – Nov. 2017

An array of 74 sensors deployed during November 4 – 25, 2017 for carrying out ambient seismic noise measurements

Observations

- One order reduction in magnitude of seismic ground motion when measured at 10 m deep compared to the surface
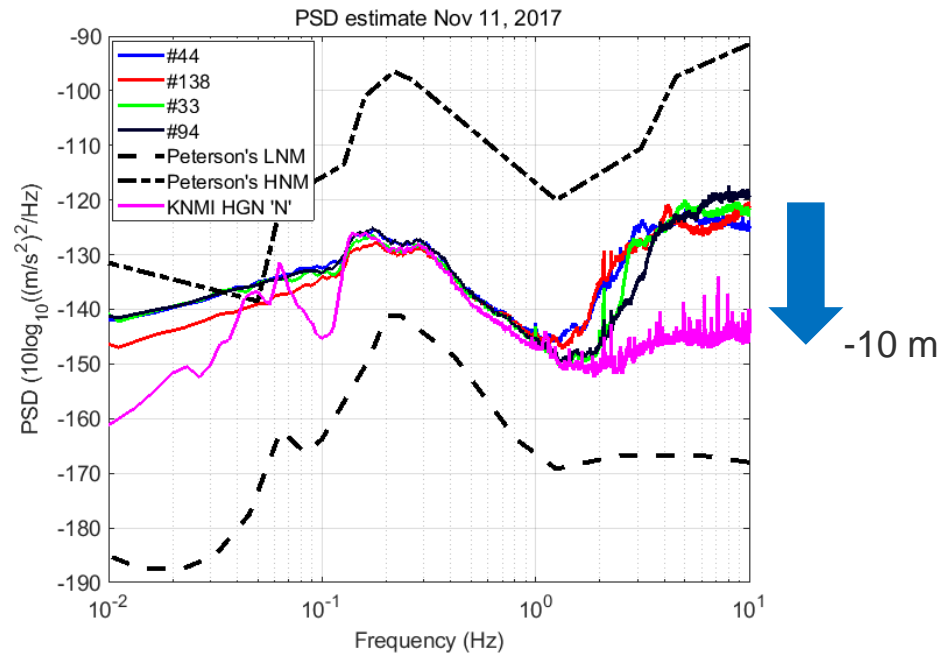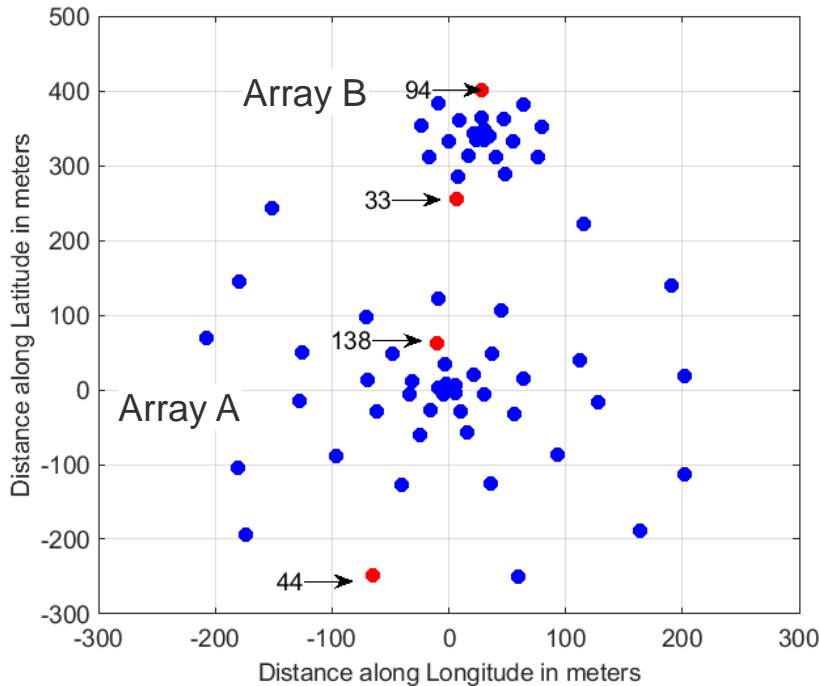
Figure 1(a) Sensor Layout, (b) Daily averaged PSD of sensors for Nov 11, 2017 marked in red

All work reported here are based on Koley et al., 2018

Beamforming output

Beamforming results show the dominant seismic wave propagation in the form of Rayleigh waves with higher order modes at frequencies greater than 5.4 Hz

Observations

- Higher order modes observed at frequencies greater than 5.4 Hz implying a sharp velocity contrast at a shallow depth

- Anisotropic illumination at low frequencies. Source distribution tend to be isotropic at high frequencies
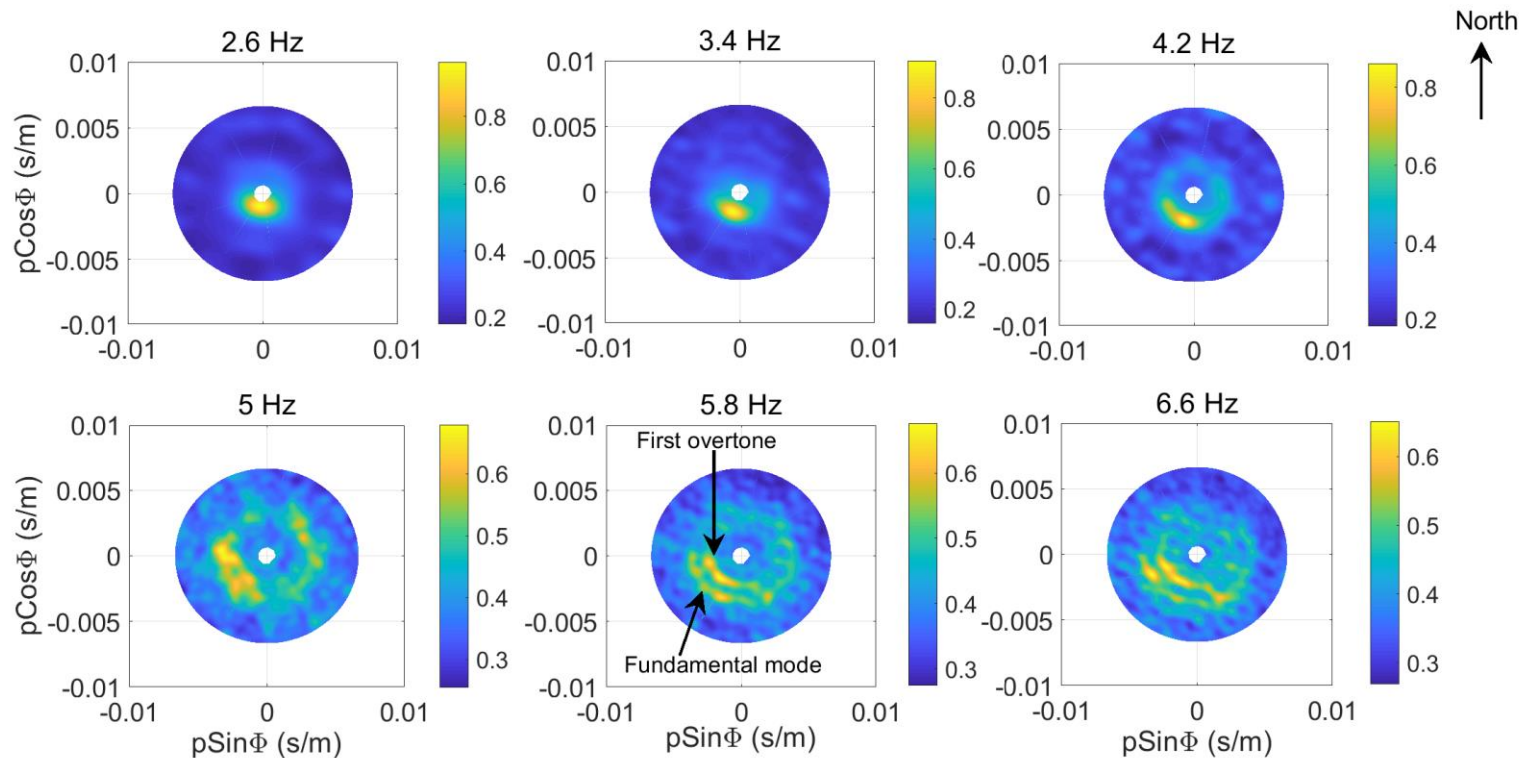

Figure 2. Beampower represented in a polar plot with azimuth measured clockwise wrt North and slowness increasing radially outwards

skoley@nikhef.nl

All work reported here are based on Koley et al., 2018

Observed Rayleigh wave phase velocity

Rayleigh wave velocities show a sharp drop from about 1000 m/s to 400 m/s between 2.5 and 4 Hz; implying a drastic change in subsurface velocities at shallow depth

Observations

- Higher order modes phase velocity derived for array with higher aperture of about 512 m
- Higher order modes not recovered for the smaller array aperture of about 220 m
    - Depth to hard rock increases
    - Too close to the seismic source for higher modes to be generated
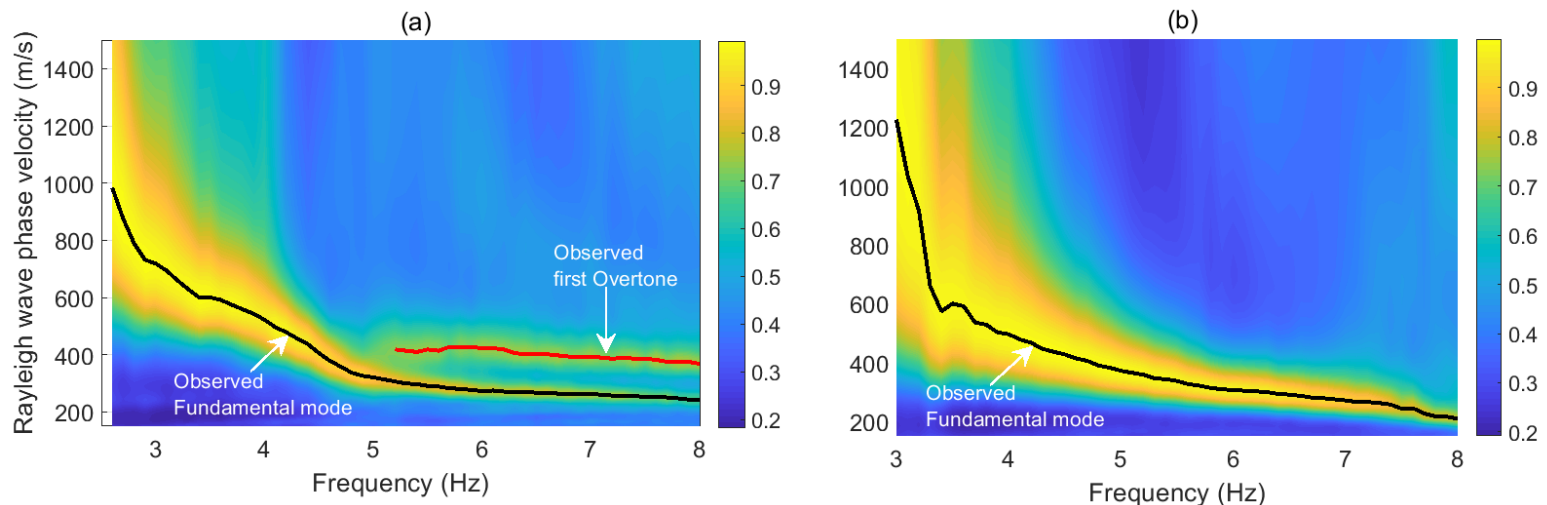
Figure 3(a) Rayleigh wave phase velocity obtained from Array A. (b) same as (a) but for Array B. No higher order modes are recovered for Array B

All work reported here are based on Koley et al., 2018

A priori subsurface information

Resistivity logging, gamma ray loging and sonic logging were performed to get a priori subsurface information which is necessary for setting the constraints for inversion

All work reported here are based on Phd Thesis M.Bader, VU Amsterdam

1D S-wave velocity model at Terziet

A transition from soft soil to hard rock is observed at depths between 35 and 50 m

Observations

- As stated earlier, the depth to bedrock is higher for Array B as shown in Fig. 4 (right)

- Velocity contrast between soft soil and hard rock is also higher beneath Array A

- The geology in the region varies significantly between points and hence a need to perform 2D or 3D modeling

Figure 4. Left: 1D S-wave velocity models derived from Array A. Right: S-wave velocity models derived from Array B

skoley@nikhef.nl

All work reported here are based on Koley et al., 2018

Active seismic survey

Active seismic survey was performed to obtain a P-wave velocity model of the subsurface along two different reciever lines which were separated by a distance of about 50 m

Survey attributes

- Receiver spacing of 3 m, and source spacing of 6 m within the the receiver array

- A total of 248 and 220 source points for Receiver line A and Receiver line B, respectively. Maximum source-receiver offset of about 953 and 776 m, respectively
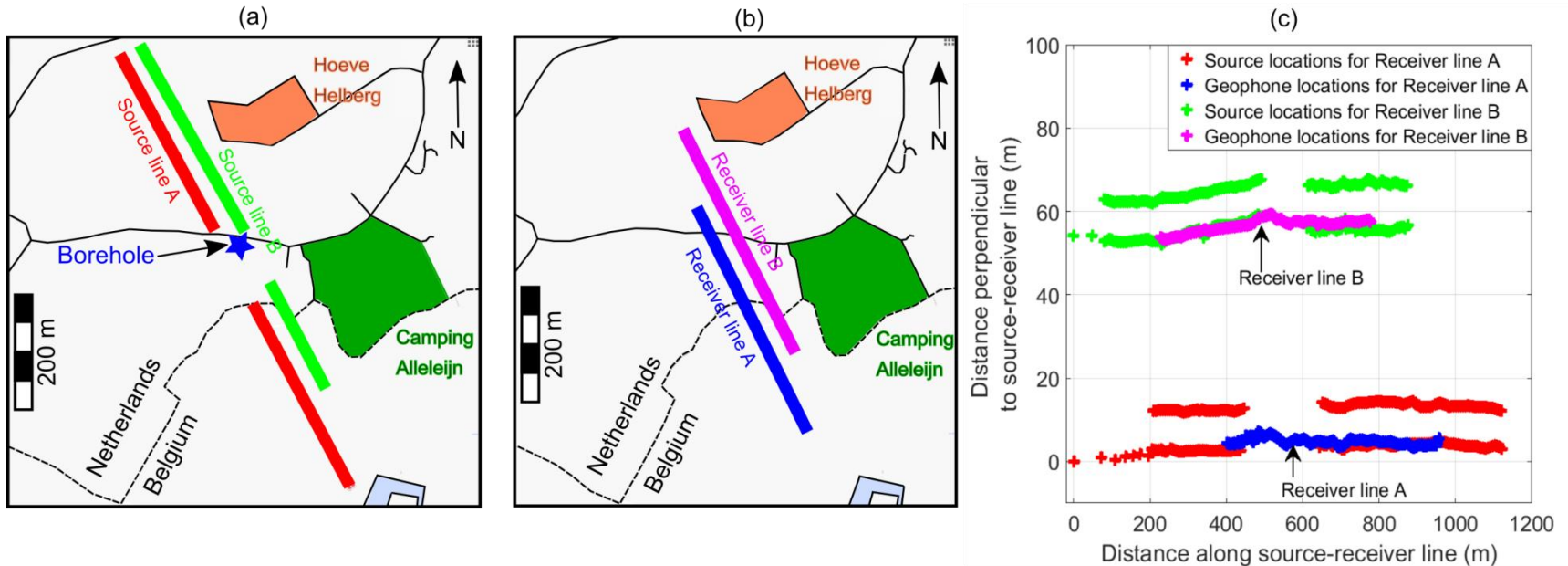

Figure 5. (a) Seismic shot lines shown in a map of the region. Each of the red and the green lines correspond to a particular receiver line. (b) Receiver lines A(blue) and B(magenta) separated by a distance of about 50 m. (c) Shot and receiver line layout shown in Cartesian coordinates

Refraction seismic tomography

2D subsurface P-wave velocity models derived from Wavepath Eikonal Tomography of refraction travel-times corresponding to the two receiver lines depict the presence of an overthrust fault at the site

Survey attributes

- Transition from soft-soil to hard rock occurs at a much shallower depth towards the left (North) and is consistent with passive seismic predictions

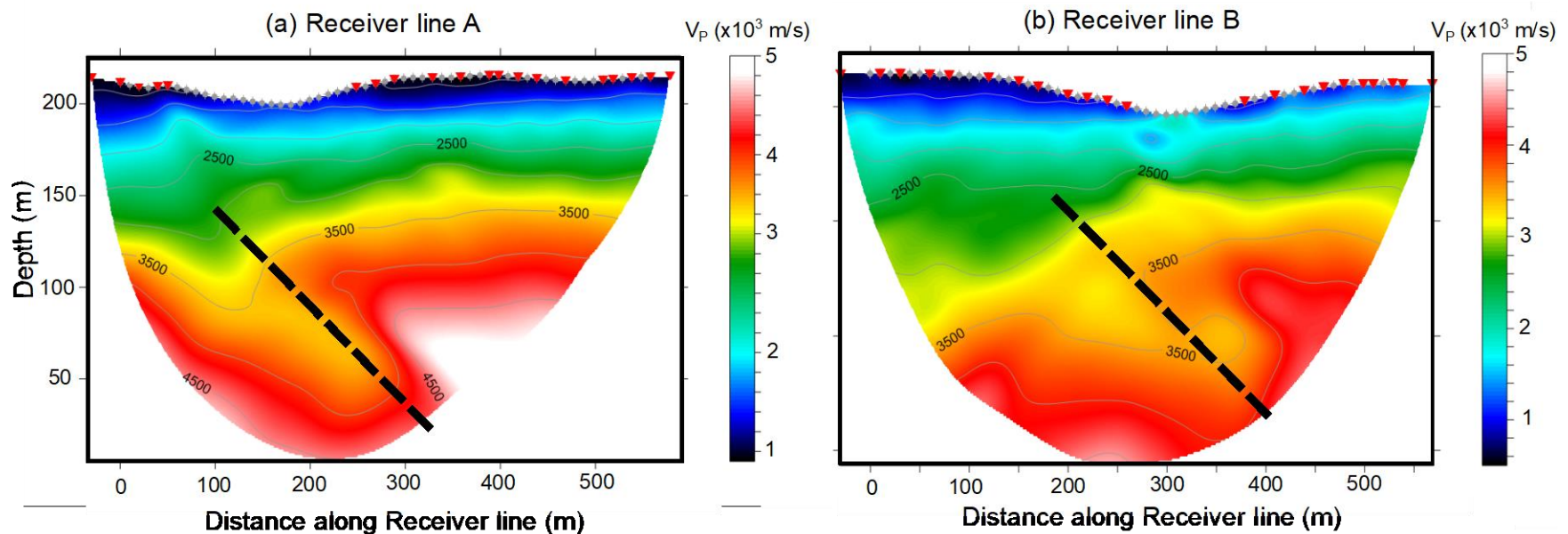- A lateral continuity is observed in the two images

Figure 6(a) WET P-wave velocity model beneath Receiver line A. (b) WET P-wave velocity model beneath Receiver line B. The dotted lines show the expected dip of the overthrust fault

All work reported here are based on Phd Thesis S. Koley, VU Amsterdam

Underground seismic noise – Nov. 2019 to Oct. 2020

We characterize the underground and the surface seismic environment by using an Streckeisen STS-5A seismometer stationed at a depth of 250 m and a Nanometrics Trillium-240 seismometer, respectively

Noise attributes

- H-V ratio: About **7** peaked at 4 Hz

- Sharp spectral noise lines observed at at frequencies of 2.1, 2.3, 3.1, 6.3, and 6.7 Hz
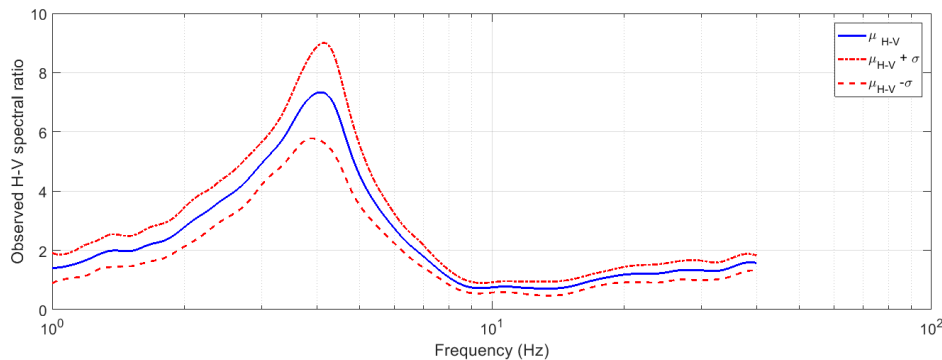

Figure 7: Mean H-V spectral ratio is shown as the blue curve and the red dotted and the solid curves show one standard deviation
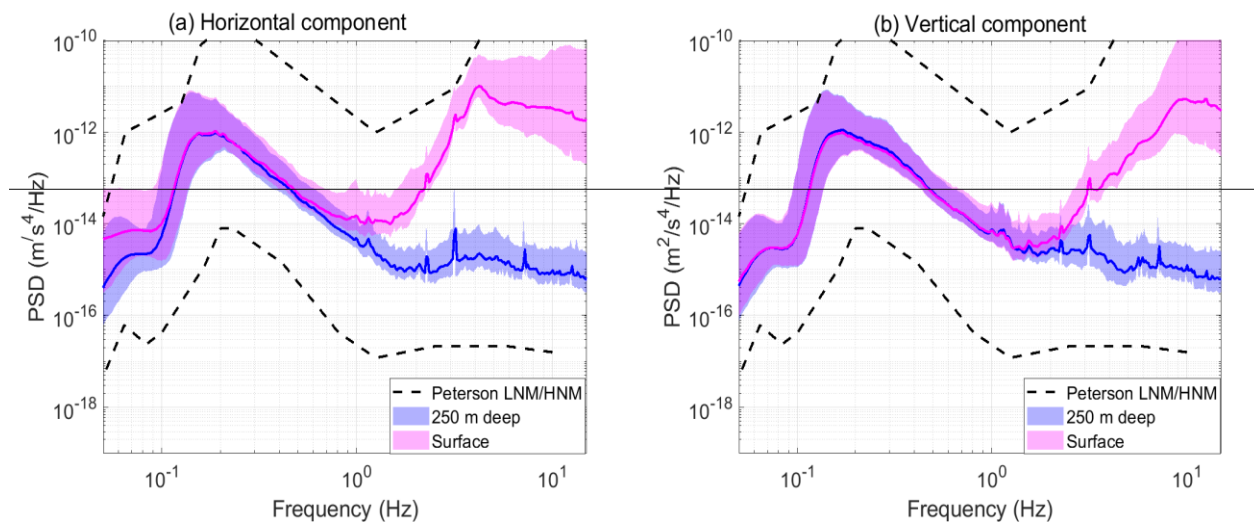

Figure 8(a) The magenta and the blue curves show the mean PSD measured between Nov., 2019 and Oct., 2020 on the surface and underground, respectively. The shaded regions correspond to the 10th and the 90th percentiles of the measurements. (b) same as (a) but for the vertical component of the seismic noise. Peterson's low noise model (LNM) and high noise model (HNM) are plotted for comparison with global observations

Underground seismic noise: microseismic variation

The average vertical and horizontal component PSD in the band 0.1 to 0.5 Hz reduces by an order of magnitude during the summer compared to winter months

Noise attributes

- Stutzmann et al., 2009 studied that microseismic noise is reduced during summer when compared to winter, and similar observations are made at Terziet
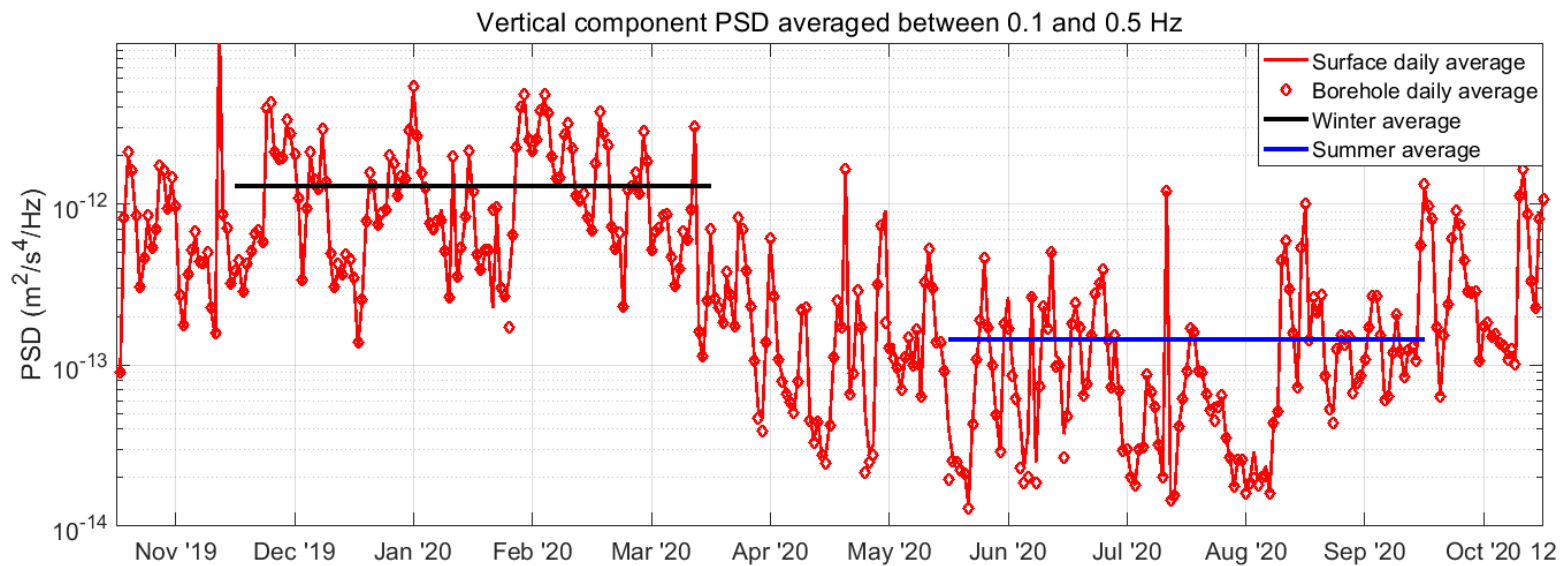

Figure 9. Temporal variation of the vertical component of the seismic noise PSD averaged in the frequency band 0.1 to 0.5 Hz. the red dots and dashed curve represent the surface and underground measurements, respectively. The horizontal black and blue lines represent the average PSD during Summer and Winter months, respectively

Underground seismic noise: anthropogenic variation

For frequencies greater than 1.5 Hz, seismic noise is attenuated when going underground by about a factor 10^4 in power

Noise attributes

- The noise measured **on the surface shows a strong day and night variation**, with the seismic noise PSD during the night showing a reduction of over **two orders of magnitude** compared to that during the day

- On the contrary the underground noise measurements during night show only a reduction in seismic noise PSD by a **factor 3 to 4** compared to that during the day. Fig. 10(b) shows the diurnal variation and a further reduction in underground seismic noise during weekends
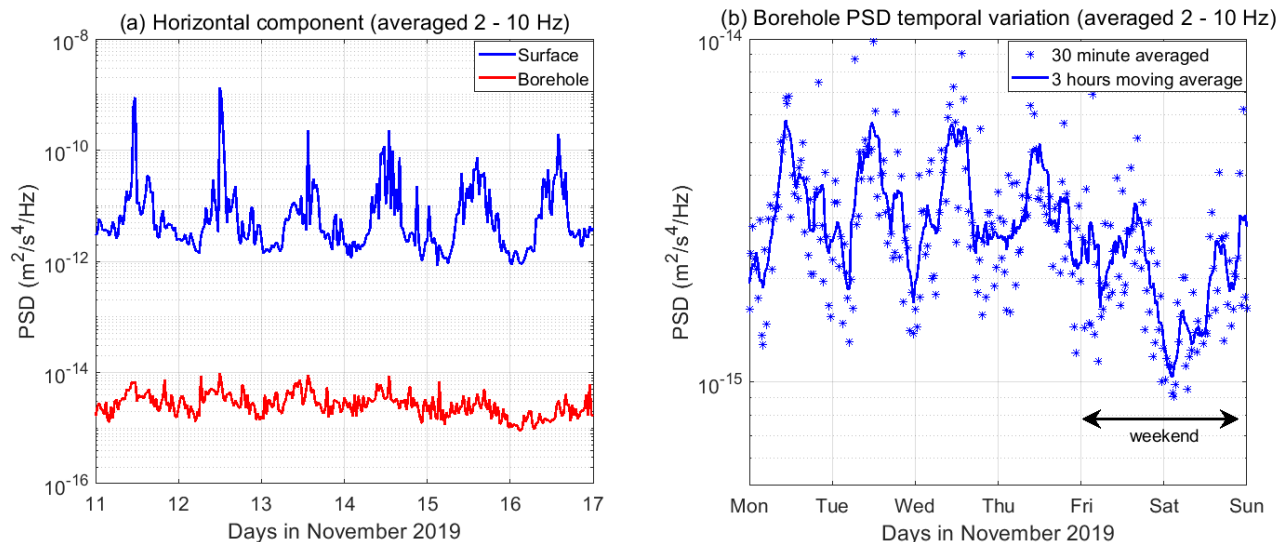

Figure 10(a) Temporal variation of the horizontal component of the ambient seismic noise PSD averaged in the frequency band 2 to 10 Hz for the time period November 11 to 17, 2019. The red and blue curves represent the surface and the underground measurements, respectively. Strong diurnal variation is observed for the surface noise. (b) Diurnal variation by only a factor of 3-4 is observed for the underground seismic noise. A further reduction by a factor 2 is observed during weekends when compared to that during weekdays

Underground seismic noise: attenuation

The geology at Terziet is well suited to attenuate seismic noise created on the surface

Observations

- Attenuation between surface and underground seismic noise for frequencies **up to 4 Hz is about the same during day and night**, since for this frequency band the ambient seismic noise is dominated by surface waves

- Beyond 4 Hz, the contribution of surface waves to the underground seismic noise reduces drastically. This is evident from the flat trend of the attenuation curves shown in Fig. 11. Attenuation of seismic noise for these frequencies is about 10^4 in power. Overall, the attenuation in seismic noise power is smaller during night than during the day
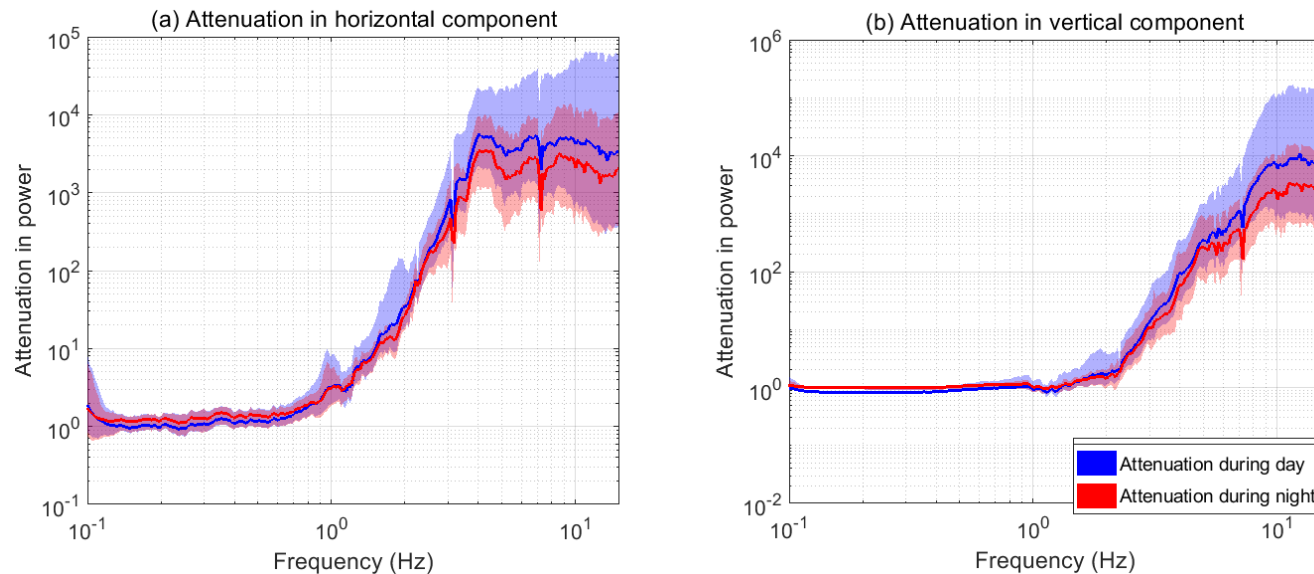

Figure 11(a) The blue and red curves show the attenuation in seismic noise power during day and night, respectively. The shaded regions show the 10th and the 90th percentile of the estimates for an year of measurement (Nov. 2019 - Oct. 2020). (b) same as (a), but for vertical component

Underground seismic noise: body wave background

At frequencies greater than 4 Hz the underground seismic noise during night is significantly higher than what would be expected if there were only surface waves, we hypothesize that the underground seismic noise is a combination of reduced surface seismic noise and background body waves

Total seismic noise underground

$$PSD(f)_{\text{depth}} = PSD(f)_{\text{surface}}\alpha(f) + \beta(f),$$

- Where $\beta(f)$ is the body wave background

- Body wave background contributes to about half of the total seismic noise at a depth of 250 m
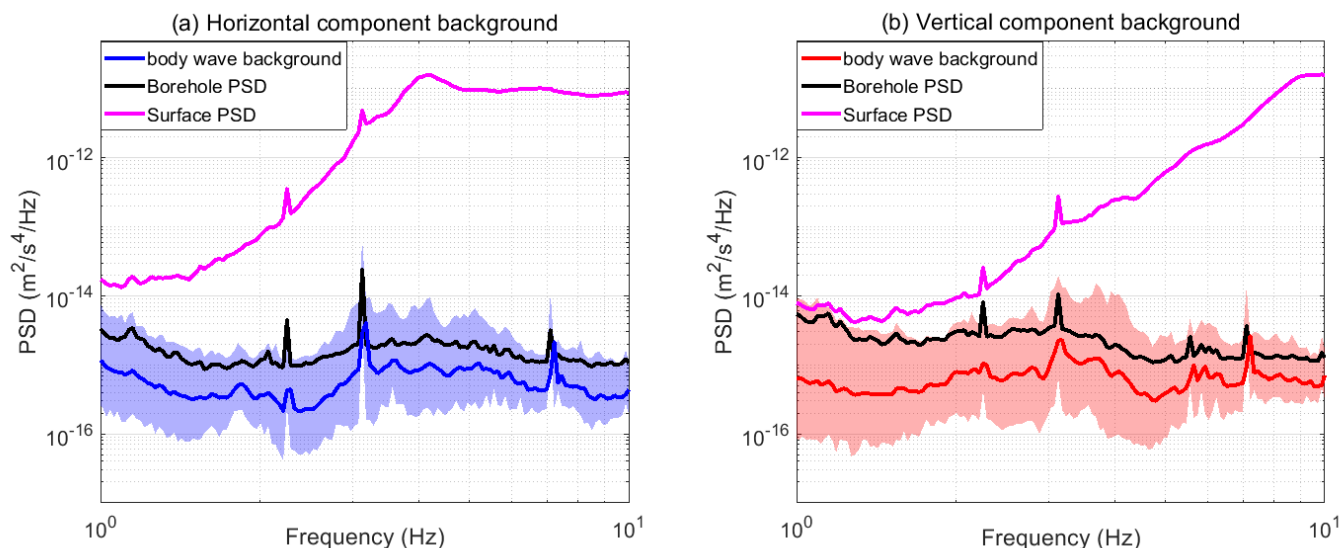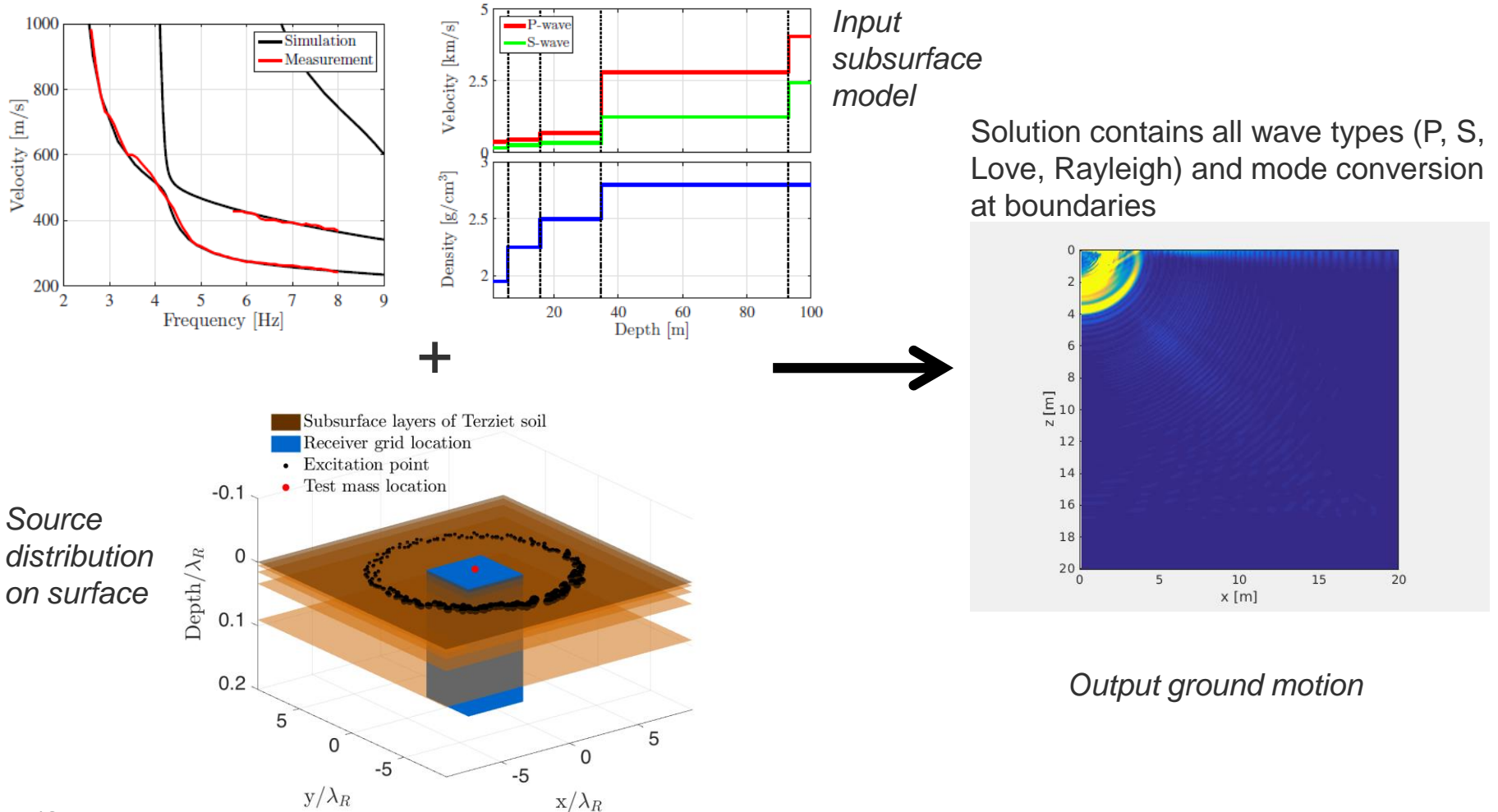

Figure 12(a) PSD of the body wave background corresponding to the horizontal component of seismic noise. The magenta and black curves correspond to the measured seismic noise measured on the surface and underground, respectively. The shaded region shown the 10th and 90th percentiles over all analysis windows. (b) Same as (a) but for the vertical component

Towards modeling Newtonian noise

The first step is simulating the seismic motion of the elements in a volume surroundng the test-mass

Using EDT elastodynamic solver to simulate the ground motion:

Input subsurface model

Solution contains all wave types (P, S, Love, Rayleigh) and mode conversion at boundaries

+

Source distribution on surface

Output ground motion

All work reported here are based on Phd Thesis M.Bader, VU Amsterdam

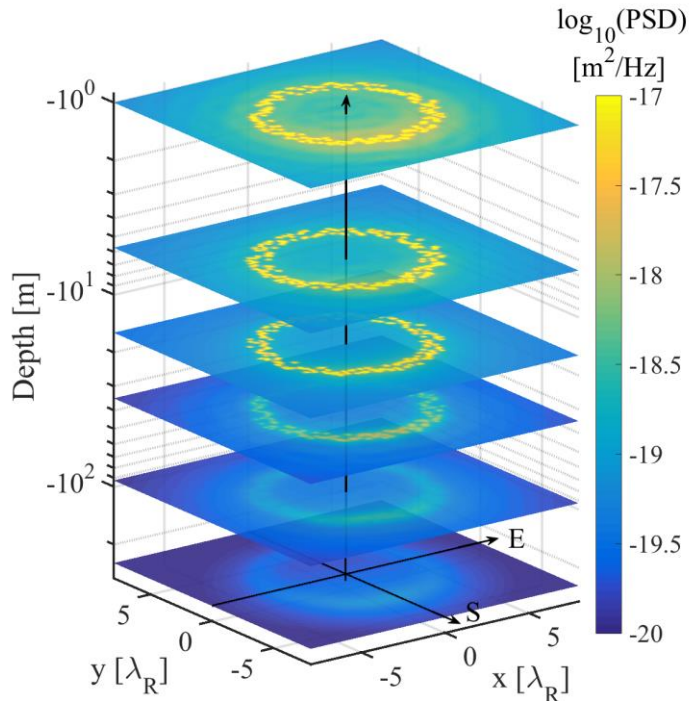# Modeling Newtonian noise: simulated ground motion

Figure 13: Model of displacement noise that reproduces the measured surface PSD at 2.6 Hz. The first five sheets show the PSD across the top surface of each new layer. The sheet at 250 meter depth shows the PSD near the test mass. Note the strong amplitude reduction at depths greater than 35 meter, where the hard rock layer begins
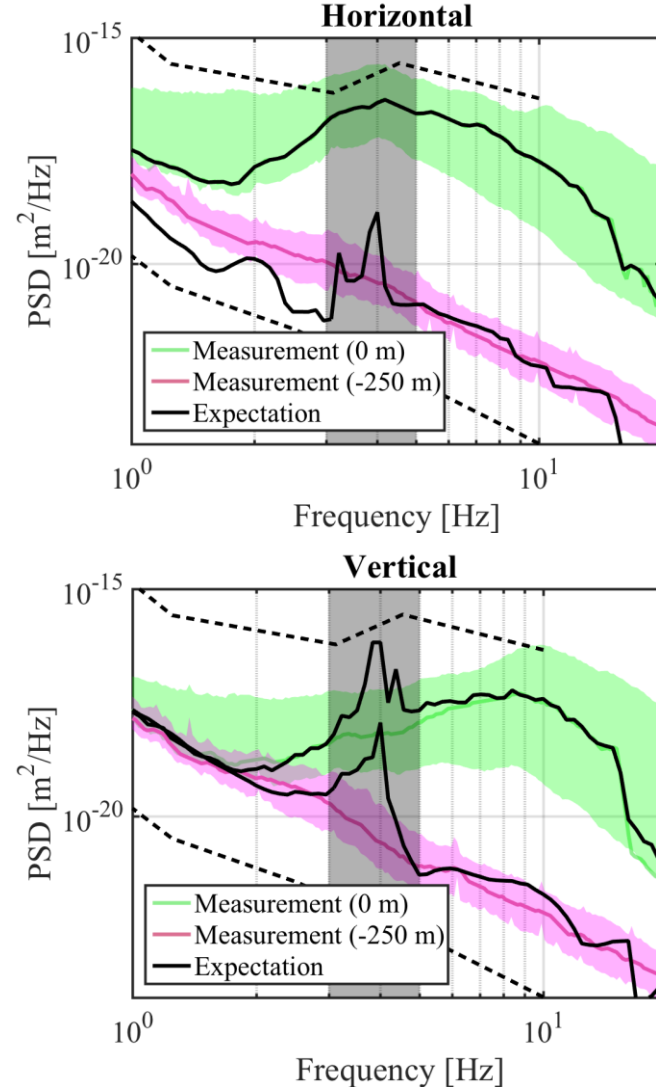

Figure 14: Simulated vs observed horizontal and vertical ground motion on the surface and at depth

All work reported here are based on Phd Thesis M.Bader, VU Amsterdam
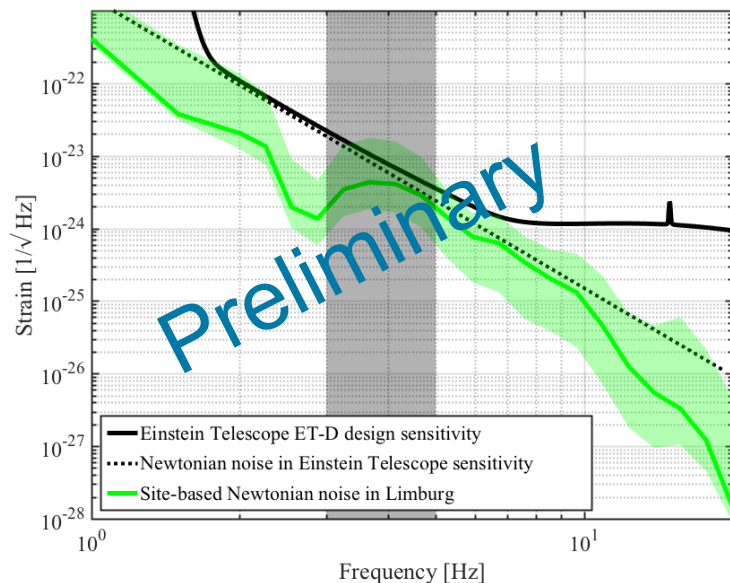
Modeled Newtonian noise

Figure 15: Modeled Newtonian noise at the BGN site. Possibly overestimated around 4 Hz where a peak in the H-V ratio is observed

Improvements:

- Understanding the source mechanism

  - Dominantly horizontal or vertical sources – Install more 3-component geophones at the site

  - Matching the observed H-V ratio around 4 Hz

- Consider the contribution of background body waves that originate from sources that are not on the surface

- Constraining the surface wave Eigenfunction by installing a string of geophones down a borehole

All work reported here are based on Phd Thesis M.Bader, VU Amsterdam

Questions?

References

- Processing seismic ambient noise data to obtain reliable broad-band surface wave dispersion measurements, G. D. Bensen[1], M. H. Ritzwoller[1], M. P. Barmin[1], A. L. Levshin[1], F. Lin[1], M. P. Moschetti[1], N. M. Shapiro[2] and Y. Yang. Geophysical journal International, 2007.
- On a frequency-time analysis of oscillations, A.L.Levshin, V.F. Pisarenko, G.A. Pogrebinsky, Annales of Geophysics, 1972.
- Surface wave tomography of the western United States from ambient seismic noise: Rayleigh and Love wave phase velocity maps, Fan-Chi Lin, Morgan P. Moschetti and Michael H. Ritzwoller, Geophysical Jounal International, 2007.
- A Comparison of Strategies for Seismic Interferometry, Roel Snieder, Masatoshi Miyazawa, Evert Slob, Ivan Vasconcelos, Kees Wapenaar, Survey Geophysics, 2009.
- Extracting the Green's function from the correlation of coda waves: A derivation based on stationary phase, Roel Snieder, Physical review E, 2004.
- Retrieving the Green's function in an open system by cross correlation: A comparison of approaches (L) Kees Wapenaar and Jacob Fokkema Department of Geotechnology, Delft University of Technology, Delft, The Netherlands Roel Snieder Center for Wave Phenomena, Colorado School of Mines, Golden, Colorado 80401, Acoustic Society of America, 2005.
- On measuring surface wave phase velocity from station–station cross-correlation of ambient signal, Boschi, Lapo; Weemstra, Cornelis; Verbeke, Julie; Ekström, Göran; Zunino, Andrea; Giardini, Domenico, Geophysical Journal International, 2012.
- Spectral Whitening in the Frequency Domain, M. W. Lee, Open-File Report 86-108, U.S Geological survey.
- A fast and reliable method for surface wave tomography, M.P. Barmin, M.H. Ritzwoller, A.L. Levshin, Pure and Applied Geophysics, 2001.
- Basic Principles of Wave Propagation, Gerard T. Schuster, 2011.

References

- High-resolution 3D shallow crustal structure in Long Beach, California: Application of ambient noise tomography on a dense seismic array, Fan-Chi Lin[1], Dunzhu Li[1], Robert W. Clayton[1], and Dan Hollis2, Geophysics, 2013.
- Case History: High-frequency Rayleigh-wave tomography using traffic noise from Long Beach, California Jason P. Chang[1], Sjoerd A. L. de Ridder[2], and Biondo L. Biondi[1], Geophysics, 2016.
- Surface-wave eikonal tomography for dense geophysical arrays Pierre Gouedard[1], Huajian Yao[1;2], Fabian Ernst[3], and Robert D. van der Hilst[1], [1]Earth, Atmospheric and Planetary Sciences department, Massachusetts Institute of Technology, [2]Institute of Geophysics and Planetary Physics, Scripps Institution of Oceanography, [3]Shell Projects and Technology.
- Rayleigh wave group velocities at periods of 6–23 s across Brazil from ambient noise tomography Bruno Goutorbe,[1] Diogo Luiz de Oliveira Coelho[2] and St´ephane Drouet[2], Geophysical Journal International, 2015.
- Passive seismic imaging with directive ambient noise: application to surface waves and the San Andreas Fault in Parkfield, CA, Philippe Roux, Geophysical Journal International, 2009.
- Tomographic inversion via the conjugate gradient method John A. Scales*, Geophysics, 1987.
- Traveltime tomography: A comparison of popular methods, W. Scott Phillips* and Michael C. Fehler, Geophysics, 1991.
- Shaping regularization in geophysical-estimation problems, Sergey Fomel1, Geophysics, 2007.
- On the effect of topography on surface wave propagation in the ambient noise frequency range Andreas Köhler · Christian Weidle · Valérie Maupin, Journal of Seismology, 2011.